Schramm, Stefan; Dietzel, Alexander; Blum, Maren-Christina; Link, Dietmar; Klee, Sascha

Technical light-field setup for 3D imaging of the human nerve head validated with an eye model

Original published in:	Current directions in biomedical engineering. - Berlin : De Gruyter. - 7 (2021), 2, p. 433-436.
Conference:	Annual Meeting of the German Society of Biomedical Engineering (VDE/DGBMT) ; 55 (Hannover) : 2021.10.05-07
Original published:	2021-10-09
ISSN:	2364-5504
DOI:	10.1515/cdbme-2021-2110
[*Visited:*	2022-03-07]

Stefan Schramm*, Alexander Dietzel, Maren-Christina Blum, Dietmar Link and Sascha Klee

Technical light-field setup for 3D imaging of the human nerve head validated with an eye model

Abstract: With the new technology of 3D light field (LF) imaging, fundus photography can be expanded to provide depth information. This increases the diagnostic possibilities and additionally improves image quality by digitally refocusing. To provide depth information in the human optic nerve head such as in glaucoma diagnostics, a mydriatic fundus camera was upgraded with an LF imager. The aim of the study presented here was the validation of the technical setup and resulting depth estimations with an appropriate eye model. The technical setup consisted of a mydriatic fundus camera (FF450, Carl Zeiss Meditec AG, Jena, Germany) and an LF imager (R12, Raytrix GmbH, Kiel, Germany). The field of view was set to 30°. The eye model (24.65 mm total length) consisted of a two-lens optical system and interchangeable fundus models with papilla excavations from 0.2 to 1 mm in steps of 0.2 mm. They were coated with red acrylic lacquer and vessels were drawn with a thin brush. 15 images were taken for each papilla depth illuminated with green light (wavelength 520 nm ± 20 nm). Papilla depth was measured from the papilla ground to the surrounding flat region. All 15 measurements for each papilla depth were averaged and compared to the printed depth. It was possible to perform 3D fundus imaging in an eye model by means of a novel LF-based optical setup. All LF images could be digitally refocused subsequently. Depth estimation in the eye model was successfully performed over a 30° field of view. The measured virtual depth and the printed model papilla depth is linear correlated. The presented LF setup allowed high-quality 3D one-shot imaging and depth estimation of the optic nerve head in an eye model.

Keywords: light-field, fundus imaging, papilla, eye model

https://doi.org/10.1515/cdbme-2021-2110

1 Introduction

Classical fundus photography is an established and fast method for diagnosis and documentation of retinal diseases. In contrast to current scanning methods like scanning laser ophthalmoscopy or optical coherence tomography, it offers only 2D information of the fundus. The new light field (LF) technologies offer the possibility to capture an 3D image in one shot [1]. Additionally, the image quality can be improved subsequently by digitally refocusing [2]. In particular, the acquisition of 3D information provides depth information that can increase diagnostic capabilities of the fundus photography, e.g., for glaucoma diagnosis.

One strong risk factor for glaucoma is a suspicious optic nerve head appearance with an abnormal cupping or an increase in the cup-to-disc ratio [3,4] with an increase in papillary depth accompanied by steeper excavation walls, which is measurable in 3D space. With demographic change in the industrialized countries, the incidence of glaucoma is increasing. As this eye disease is one of the most common causes of blindness [5,6], cost-effective, rapid and safe screening is a key factor in rapid medical intervention.

Other authors have already shown that light field fundus photography on the human eye is possible in principle, but they use their own designed fundus cameras with simple optics. The image quality therefore does not permit a useful depth estimate. [7–9]

Our approach is to equip a standard fundus camera with a light field imager to determine the depth of the papilla. To validate the technical setup and the depth estimation, an eye model with

*Corresponding author: Stefan Schramm: Institute of Biomedical Engineering and Informatics, Faculty of Computer Sciences and Automation, Technische Universität Ilmenau, Ilmenau, Germany, stefan.schramm@tu-ilmenau.de

Alexander Dietzel, Maren-Christina Blum, Dietmar Link: Institute of Biomedical Engineering and Informatics, Faculty of Computer Sciences and Automation, Technische Universität Ilmenau, Ilmenau, Germany

Sascha Klee: Department of General Health Studies, Division Biostatistics and Data Science, Karl Landsteiner University of Health Sciences, Krems an der Donau, Austria, sascha.klee@kl.ac.at; Institute of Biomedical Engineering and Informatics, Faculty of Computer Sciences and Automation, Technische Universität Ilmenau, Ilmenau, Germany

interchangeable fundus models regarding different papilla depths was designed and realized to perform a study.

2 Methods

2.1 Eye Model

The main aspects that the eye model should address are the modelling of the back reflections of the cornea and the internal reflections, a size ratio to the real human eye of 1:1 and the interchangeability of the fundus with different papillary depths. Therefore, the design starting point was the radius of the corneal anterior surface with 7.707 mm and the requirement for a two-lens system to generate a correspondingly large number of reflections. The optical transmission properties should be similar to those of the human eye. Figure 1 shows the resulting eye model with a total length of 24.65 mm from the cornea anterior surface to the fundus surface in an isometric and a sectional view. The optical parameters are listed in Table 1.

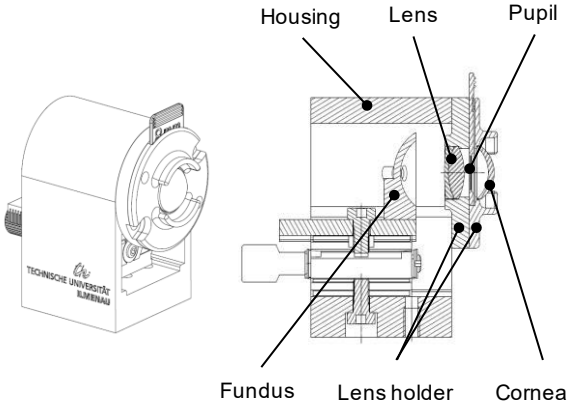

Figure 1: Isometric view of the eye model (left) and a sectional view of the eye model (right) showing the parts of the eye model (linear translation stage for focus adjustment and screws are not labeled for clarity).

Lens holder for the cornea model and lens model as well as the housing and the fundus models were 3D-printed with a resolution of 25 µm on an Objet30 Prime printer (Stratasys Ltd, Eden Prairie, USA) with white plastic (VeroWhiteTM, Stratasys Ltd, Eden Prairie, USA). The fundus models were coated with red acrylic lacquer (MolotowTM, Feuerstein GmbH, Lahr, Germany), and vessels were hand drawn with a thin brush with black acrylic lacquer.

To estimate the optical performance of the eye model, the Modulus of the optical transfer function (MTF) of the eye model was calculated with Zemax OpticStudio® (Version 21.1.1, Zemax Europe, Ltd., Stansted, United Kingdom) Figure 2 shows the resulting MTF of the eye model in comparison to the measured MTF of Guirao et al. 1999. He measured the MTF of the human eye as a function of age [10]. With a pupil diameter of 4 mm the eye model fits the measured MTF of the age group of 40 – 50 years best.

Table 1: Surfaces of the eye model with its radius, distance to the next surface and material.

Surface	Radius (mm)	Distance (mm)	Material
Cornea Front	7.707		
		1.5	N-BK7
Cornea Back	8.886		
		4.5	Air
Pupil	-		
		1.5	Air
Lens Front	14.288		
		4	N-LAK10
Lens internal	-13.762		
		1	N-SF57
Lens Back	-68.516		
		12.15	Air
Fundus	-10		

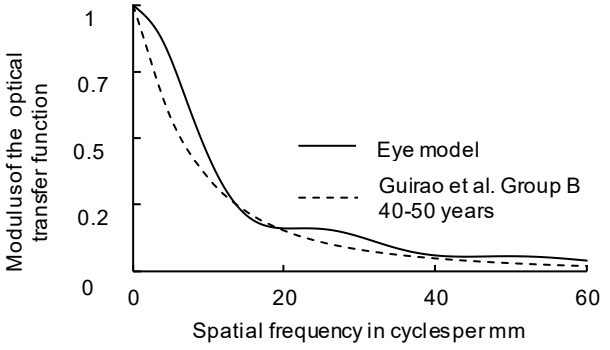

Figure 2: Comparison of the simulated Modulus of the optical transfer function (MTF) (solid line) at 0° with 4 mm pupil-diameter with the measured MTF from Guiaro et al. 1999 for Group B 40 - 50 years (dashed line). The simulated MTF slightly overestimates the measured MTF in parts.

2.2 Technical Setup

The technical setup consisted of three main parts: a fundus camera (FF450, Carl Zeiss Meditec AG, Jena, Germany), an LF imager (R12, Raytrix GmbH, Kiel, Germany) connected with an c-mount adapter and the Raytrix LF software (RxLive 5.0.046.0, Raytrix GmbH, Kiel, Germany).

The fundus camera is a standard device with an illumination wavelength of 520 nm ± 20 nm. The field of view of the fundus camera was set to 30°. The f-number of the aperture of the fundus camera can be estimated with 5.6.

The LF imager consists of a microlens array (f-number = 2.4) with lenses in a hexagonal grid of three focal lengths and a 16-bit monochrome half-inch sensor with a maximum framerate of 29 frames per second. This setup corresponds to an LF camera type two [2,11].

The LF imager is operated with its specific LF software which is also used for depth estimations.

2.3 Imaging procedure and measurement analysis

For each papilla depth 15 images were taken. The camera was readjusted with every image capture including the illumination intensity and exposure parameters of the LF imager. The image brightness was adjusted so that the papilla, which is the brightest area of the image, was at the limit of saturation.

The local depth was determined by averaging over a circular region. The diameter of this region was according to the complete bottom of the papilla and kept constant for all measurements. The papilla depth was then determined as the difference between the flat surrounding region and the bottom of the papilla.

All 15 measurements for each papilla depth were averaged and used for a linear regression with the real model papilla depths.

Since the LF system is not metrically calibrated, the measurements are given in virtual mm.(v-mm).

3 Results

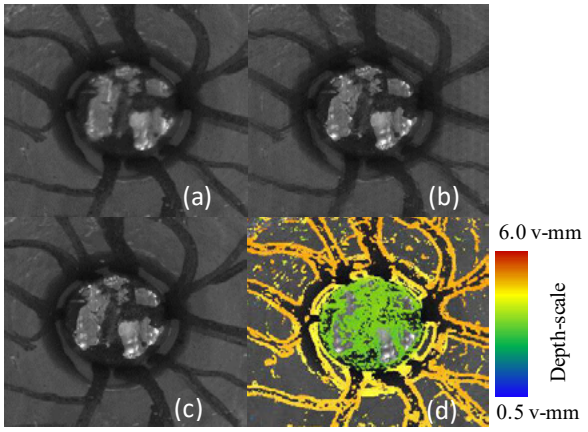

Figure 3: Refocused partial images (approx. 10° field of view) of the eye model papilla with 0.8 mm depth (a): retina focused; (b): papilla bottom focused; (c): total focus image with maximum depth of focus; (d): total focus image with depth map overlay, green color indicating low regions, orange indicating high regions.

3D fundus imaging with die novel LF-based optical setups in the here presented eye model was possible for all papilla depths. Figure 3 shows refocused partial images with an approximate 10° field of view of an eye model papilla with 0.8 mm depth. Refocusing on the retina (Figure 3 (a)) and on the papilla ground (Figure 3 (b)) was possible for all images. Also, the generation of a total focus image with a maximum depth of focus (Figure 3 (c)) was possible for all taken images.

Depth estimation was successfully performed for all papilla depths over a 30° field of view. Figure 4 shows boxplots for each papilla depth and the linear correlation between the estimated virtual depth in v-mm and the real eye model papilla depth in mm. The narrow boxes indicate a good repeatability of the measurement. The linear fit has only a small negligible offset.

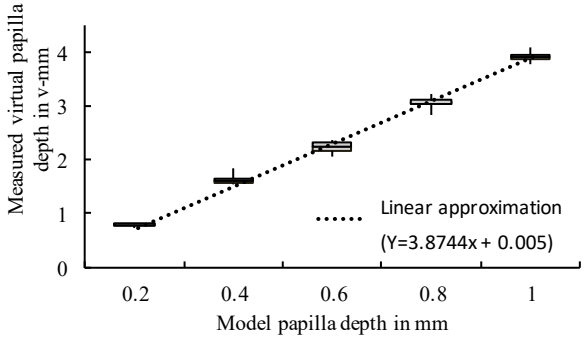

Figure 4: Relationship between the measured depth of the papilla in v-mm and the depth of the papilla in the eye model in mm. The boxplots represent the distribution of model papilla depths over n = 15 LF measurements per fundus model. Dotted line: linear fit with Y = measured virtual papilla depth and x = model papilla depth.

4 Discussion

In the eye model study presented here, we have shown that depth estimation at the papilla with an LF fundus camera is possible in principle. Subsequent digital image enhancement by refocusing and total focus generation was possible for all images and represents a clear benefit for fundus photography.

A depth estimation was also possible for all images. The linear regression mapped the measurements well, indicating a linear relationship. With the good correlation to the real depth of the fundus model and low scatter of the estimated depth values, the method of papilla depth estimation is valid. In addition, the low value dispersion indicates good reproducibility. To obtain a realistic order of magnitude, the next step is to metrically calibrate the entire system including the software with its parameters specific to LF fundus imaging. In addition, further parameters, such as angle of the excavation walls or a cup-to-disk ratio equivalent, regarding early glaucoma detection can be implemented.

The eye model used here has good optical performance on the optical axis. However, with the design requirements set, it does not model all the optical properties of the human eye. Many other eye models presented in the literature include specific aspects of optical imaging with corresponding model complexity [12–15]. If it is possible to reproduce typical aberrations of the human eye in the model and to integrate a dimensional scale, a metric model-based calibration can be performed with it.

Thus, the integration of the LF technology can be a future-oriented extension of classical fundus photography.

Author Statement

Research funding: The author state no funding involved. Conflict of interest: Authors state no conflict of interest.

References

[1] Ulrich Perwass, Christian Perwass. Digital imaging system, plenoptic optical device and image data processing method. US2012/0050562A1, 2012.

[2] Lumsdaine A, Georgiev T. The focused plenoptic camera. 2009 IEEE International Conference on Computational Photography (ICCP), San Francisco, CA, USA: IEEE; 2009, p. 1–8. https://doi.org/10.1109/ICCPHOT.2009.5559008.

[3] Veena HN, Muruganandham A, Kumaran TS. A Review on the optic disc and optic cup segmentation and classification approaches over retinal fundus images for detection of glaucoma. SN Applied Sciences 2020;2:1476. https://doi.org/10.1007/s42452-020-03221-z.

[4] Seema Thakur, Neha Srivastava, Deepshikha Patle. Glaucoma : A Review. Current Trends in Biotechnology and Pharmacy 2020;14:217–28. https://doi.org/10.5530/ctbp.2020.2.22.

[5] Tham Y-C, Li X, Wong TY, Quigley HA, Aung T, Cheng C-Y. Global Prevalence of Glaucoma and Projections of Glaucoma Burden through 2040. Ophthalmology 2014;121:2081–90. https://doi.org/10.1016/j.ophtha.2014.05.013.

[6] David S. Friedman. Prevalence of Open-Angle Glaucoma Among Adults in the United States. Arch Ophthalmol 2004;122:532–8. https://doi.org/10.1001/archopht.122.4.532.

[7] Palmer DW, Thomas Coppin, Krishan Rana, Donald G. Dansereau, Marwan Suheimat, Michelle Maynard, et al. Glare-free retinal imaging using a portable light field fundus camera. Biomedical Optics Express 2018;9:3178–92. https://doi.org/10.1364/BOE.9.003178.

[8] Alexandre R. Tumlinson, Matthew J. Everett. Light field camera for fundus photography. US8,998,411B2, 2015.

[9] Bloch E, Thurin B, Keane P, Nousias S, Bergeles C, Ourselin S. Retinal fundus imaging with a plenoptic sensor. In: Manns F, Söderberg PG, Ho A, editors. Ophthalmic Technologies XXVIII, San Francisco, United States: SPIE; 2018, p. 81. https://doi.org/10.1117/12.2286448.

[10] Guirao A, Gonzalez C, Redondo M, Geraghty E, Norrby S, Artal P. Average Optical Performance of the Human Eye as a Function of Age in a Normal Population n.d.:11.

[11] Zhu S, Lai A, Eaton K, Jin P, Gao L. On the fundamental comparison between unfocused and focused light field cameras. Appl Opt 2018;57:A1–11. https://doi.org/10.1364/AO.57.0000A1.

[12] Arianpour A, Tremblay E, Stamenov I, Ford J, Schanzlin D, Lo Y. An optomechanical model eye for ophthalmological refractive studies. Journal of Refractive Surgery 2013;29 2:126–32.

[13] Drauschke A. Comparison of Numerical Eye Models and its Representation within a Mechanical Eye Model**The project is funded by the Municipal Department 23 – Economic Affairs, Labour and Statistics – City of Vienna within the project Laser & Optics in Applied Life Sciences (LOALiS). IFAC-PapersOnLine 2016;49:133–8. https://doi.org/10.1016/j.ifacol.2016.12.023.

[14] Drauschke A, Rank E, Traxler L, Lux K, Krutzler C. Mechanical Eye Model for Comparison of Optical and Physiological Imaging Properties. IFAC Proceedings Volumes 2013;46:1–12. https://doi.org/10.3182/20130925-3-CZ-3023.00064.

[15] Polans J, Jaeken B, McNabb RP, Artal P, Izatt JA. Wide-field optical model of the human eye with asymmetrically tilted and decentered lens that reproduces measured ocular aberrations. Optica 2015;2:124. https://doi.org/10.1364/OPTICA.2.000124.